Investigating the role of microbes in mineral weathering: Nanometre-scale characterisation of the cell-mineral interface using FIB and TEM

Michael B. Ward[a*], Dana Kapitulčinová[b,c,f], Andrew P. Brown[a], Peter J. Heard[d], David Cherns[c], Charles S. Cockell[e], Keith R. Hallam[d], K. Vala Ragnarsdóttir[b,f]

[a]Institute for Materials Research, School of Process, Environmental and Materials Engineering, University of Leeds, Leeds, LS2 9JT, UK

[b]School of Earth Sciences, University of Bristol, Bristol, BS8 1RJ, UK

[c]School of Physics, University of Bristol, Bristol, BS8 1TL, UK

[d]Interface Analysis Centre, University of Bristol, Bristol, BS2 8BS, UK

[e]CEPSAR, Open University, Milton Keynes, MK7 6AA, UK

[f]Institute of Earth Sciences, School of Engineering and Natural Sciences, University of Iceland, Askja, 101 Reykjavík, Iceland

*For correspondence: E-mail m.b.ward@leeds.ac.uk; Tel. +44 113 343 2559; Fax +44 113 343 2384; current postal address: Engineering Building, University of Leeds, Clarendon Road, Leeds, LS2 9JT, UK.

1

Abstract

Focused ion beam (FIB) sample preparation in combination with subsequent transmission electron microscopy (TEM) analysis are powerful tools for nanometre-scale examination of the cell-mineral interface in bio-geological samples. In this study, we used FIB-TEM to investigate the interaction between a cyanobacterium (Hassallia byssoidea) and a common sheet silicate mineral (biotite) following a laboratory-based bioweathering, incubation experiment. We discuss the FIB preparation of cross-sections of the cell mineral interface for TEM investigation. We also establish an electron fluence threshold in biotite for the transition from scanning (S)TEM electron beam induced contamination build up on the surface of biotite thin sections to mass loss, or hole-drilling within the sections. Working below this threshold fluence nanometre-scale structural and elemental information has been obtained from biotite directly underneath cyanobacterial cells incubated on the biotite for three months. No physical alteration of the biotite was detected by TEM imaging and diffraction with little or no elemental alteration detected by STEM energy dispersive X-ray (EDX) elemental line scanning nor by energy filtered TEM (EF-TEM) jump ratio elemental mapping. As such we present evidence that the cyanobacterial strain of Hassallia byssoidea did not cause any measurable alteration of biotite, within the resolution limits of the analysis techniques used, after three months of incubation on its surface.

1. Introduction

Over the past decade, understanding of the role of micro-organisms in mineral weathering has advanced considerably. Numerous studies on microbe-mineral interactions have shown that micro-organisms substantially affect the process of mineral weathering (termed "bioweathering" hereafter) (Burford et al., 2003; Gadd, 2007; Hoffland et al., 2004; Hutchens et al., 2003; Kalinowski et al., 2000). Despite this increasing evidence that microbial cells can play a major role in mineral alteration, the processes occurring at the cell-mineral interface remain poorly understood.

Transmission electron microscopy (TEM) is a technique able to examine the cell-mineral interface because of its imaging capabilities and productive history in the analysis of minerals (for a recent review see Lee (2010)). TEM requires the preparation of electron transparent

specimens and for geological materials this is typically achieved by grinding minerals to a powder, ion milling or ultra-microtome sectioning (Heaney et al., 2001; Lee, 2010). Nevertheless, these methods do not guarantee specimen preparation at specific sites of interest. The introduction of focused ion beam (FIB) milling into the field of geoscience about a decade ago brought a solution to this problem. FIB uses a high-energy gallium ion beam to cut thin-sections from a pre-imaged, and therefore site-specific, area of practically any material that is stable in the evacuated chamber of the instrument.

FIB preparation of electron-transparent specimens, or "FIB sections", from geological materials is becoming more commonplace (e.g., Wirth, 2009; Lee, 2010). The site-specific nature of FIB milling has enabled the successful preparation of electron-transparent specimens across cell-mineral interfaces (first shown by Benzerara et al., 2005; Obst et al., 2005). More recently, FIB milling in combination with scanning (S)TEM and scanning transmission X-ray microscopy (STXM) analyses has been used to measure the accelerated weathering of a sheet silicate (biotite) by ectomycorrhizal fungi (Bonneville et al., 2011, 2009).

In this study, FIB milling and subsequent TEM analysis were used to investigate biotite weathering by cyanobacteria. Cyanobacteria are photosynthetic oxygen-evolving bacteria distributed in many environments worldwide (Madigan et al., 2003), including surfaces and internal spaces of rocks (Gorbushina, 2007). It is known that cyanobacteria are capable of the alteration of some calcium containing minerals (Garcia-Pichel, 2006; Garcia-Pichel et al., 2010), however despite their common presence on rock surfaces in natural environments their potential role in silicate mineral weathering and nutrient release is at present poorly understood. Only a small number of laboratory-based studies on cyanobacterial bioweathering of silicate minerals exist and none of the studies specifically looked at the cell-mineral interface and the potential chemical changes occurring there (Brehm et al., 2005; Büdel et al., 2004; Chizhikova et al., 2009; Gorbushina and Palinska, 1999; Olsson-Francis and Cockell, 2010). As a result, here, we characterise, by analytical TEM, the physical structure and composition of the top few layers of a sheet silicate mineral, biotite with a cyanobacterium incubated on its surface for three months. In addition, this work discusses the feasibility of using FIB milling and subsequent TEM to analyse the cell-mineral interface. As such we will: (1) identify any difficulties arising during FIB specimen preparation of bio-geological interfaces; (2) indicate a threshold electron fluence for the representative measurement of biotite composition by STEM-energy dispersive X-ray (EDX) spectrometry; and (3) report on

the nanometre scale structural and chemical impact of the laboratory incubation of cyanobacteria on biotite.

2. Material and methods

2.1. Experimental setup

A laboratory experiment was performed with one cyanobacterial strain incubated on flakes of biotite, a common sheet silicate mineral. The experimental set-up was designed to mimic the situation on rocks in natural environments, where cyanobacterial cells inhabit and colonise bare mineral surfaces with limited supplies of liquid water and essential nutrients.

A filamentous cyanobacterial strain of Hassallia byssoidea (CCALA 823, HAUER 2007/1; termed Hassallia hereafter) was used in the bioweathering experiment. The strain was isolated from biotite granite in the Czech Republic and belongs to the order Nostocales. The strain was not axenic (~5% of cells in the culture were heterotrophic bacteria). However, we accepted the presence of associated bacterial cells in the experiment because analysis by TEM would probe only the mineral regions in direct contact with the cyanobacterial cells (see details in Section 2.2. and 2.3.) minimising the possibility of identifying any weathering features caused by the associated heterotrophs. The cyanobacteria were cultivated in Bold's - Basal standard medium (BBM-st; Bischoff and Bold, 1963) while modified BBM medium (BBM-mod3) was used during their incubation on the biotite. Magnesium and iron were excluded completely from this latter medium and ammonium sulphate $(NH_4)_2SO_4$ was used to supply sulphate to the cyanobacteria. The disodium salt of ethylenediaminetetraacetic acid (EDTA-Na$_2$), typically contained in BBM-st, was omitted from the modified BBM-mod3 medium to prevent possible dissolution of the mineral due to its chelating properties. Purified agar (A6686, Sigma-Aldrich, UK) was used to prepare both the BBM-st and the BBM-mod3 solid agar media.

Biotite from Norway (departmental stock, Earth Sciences, University of Bristol) was cleaved parallel to the (001) crystal surface and cut into thin flakes (~8 × 8 × 0.2-0.5 mm) with scissors and razor blades. Three biotite flakes were placed into a Petri dish (8 mm dia.) containing the BBM-mod3 medium (1.8% w/v agar). The central topmost surfaces of the flakes were inoculated with cyanobacterial filaments using a soft plastic disposable inoculating loop, so as not to physically alter (scratch) the mineral surface. The dishes were incubated in a unit fitted with fluorescent lights for 95 days (~3 months). 60 W fluorescent lamps provided 16/8 hours of light/dark intervals in the unit and a temperature of 22±1°C was

maintained. All equipment and materials used in the experiment were either obtained sterile from the supplier or sterilised by autoclaving (~120°C for 15 min).

2.2. FIB sample preparation

FIB sections were prepared from a biotite flake obtained from the bioweathering experiment described above. A FEI Strata FIB201 system with gallium source (at the Interface Analysis Centre, University of Bristol) and a FEI Nova200 NanoLab dual beam SEM/FIB (at Leeds Electron Microscopy and Spectroscopy (LEMAS) centre, University of Leeds) were used to mill sections. The biotite flake was first sputter coated with gold (~100 nm). This was for both charge reduction during SEM analysis and as a protective layer to stop irradiation damage from the focused ion beam during initial deposition of the ion-beam deposited platinum protection layer (for a description of this damage process, see Lee (2007)). However, for this study the cell itself acted as an additional protective barrier over the cell-biotite interfaces of interest. The FIB instruments were operated at 30 kV, and at beam currents between 5 and 0.05 nA. Both ex-situ lift out using a glass needle outside the microscope chamber, and in-situ lift out using a Kleindiek micromanipulator inside the chamber were employed. FIB sections were cut from different areas on the biotite flake such that they revealed a cross-section of the bacteria and mineral, and allowed the interface to be studied by TEM (Figure 1a). Cross-sections that suffered damage during preparation (as discussed later in this paper), were not used for data collection. One damage-free section was subsequently used for detailed chemical analysis of the interface.

2.3. TEM analysis

The FIB sections were examined using a Philips EM 430 TEM (School of Physics, University of Bristol), a Philips CM200 field emission gun (FEG-)TEM fitted with an Oxford Instruments ultra thin window (UTW) X-ray detector running ISIS software and a Gatan (GIF200) imaging filter, and a FEI Tecnai F20 FEG-TEM (both at LEMAS, University of Leeds). The Philips EM 430 was used for initial structural examination of the samples, while the Philips CM200 was employed for subsequent elemental analysis by scanning (S)TEM and energy dispersive X-ray (EDX) spectroscopy and electron energy loss spectrometry (EELS). The FEI Tecnai F20 was used to assess the electron fluence threshold for beam induced mass loss in the biotite. All image processing was carried out using Gatan's Digital Micrograph software.

EDX spectroscopy was used to measure the elemental profile across the interface between the cyanobacteria and biotite by line-scanning in STEM mode. This involves scanning the electron beam repeatedly over the same line, perpendicular to the interface, and collecting a signal for specific X-ray energies (corresponding to elements of interest) for each scan dwell-point. The cumulative data can then be used to measure any changes in composition.

To establish an electron intensity threshold above which irradiation by the electron beam alters the biotite, a series of different probe configurations were scanned over the biotite (Table 1). The electron intensity, or fluence, was calculated using the beam current (measured by the instrument) and the probe dimensions, with the high angle annular dark field (HAADF) imaging capability of the FEI Tecnai F20 being used for these measurements. Electron beam diameters were measured by taking an intensity profile across a HAADF image of the interface of the biotite and the cell (which can be assumed to be atomically abrupt), collected using each respective probe setting. The diameter was taken to be the width of the interface in the image and this was averaged by integrating over approximately 300 pixels along the interface. Assuming a circular probe, the probe area could then be calculated. The optimum microscope configuration used for an electron beam to record the STEM-EDX linescans presented here (Probe 4, Table 1) was also tested on a region of the biotite away from the cell interface. These test line scans involved scanning the beam over the same line, and collecting EDX spectra at time intervals up to 30 minutes total (the approximate time for an experimental dataset to be collected). Elemental quantification of these spectra (using an Oxford Instruments standardless quantification routine) showed no composition change had occurred. The linescan data were collected using a double tilt specimen holder so that the sample could be tilted 15° towards the EDX detector and then oriented around the other tilt axis so that the interface was imaged normal to the beam direction.

EELS was used for further elemental characterisation of a section. Energy filtered TEM (EF-TEM) jump ratio maps for C, Si and Fe were collected at the interface to investigate compositional variation. Producing a jump ratio map involves taking two energy filtered images, one with an energy window that sits over a specific ionisation edge, and one just before (in the background region). The post-edge image is then divided by the pre-edge image to give a background normalised, qualitative map of the elemental distribution. Jump ratios were collected using an objective aperture of 8 mrad collection semi-angle, a 20 eV energy selecting slit and pre and post edge window positions centred 10 and 10-15 eV before and after respectively the elemental edge onsets.

2.4. Processing of STEM-EDX data

In order to identify the exact cell-mineral interface in the collected linescan data and to determine whether there was any elemental depletion in the mineral underneath the cell, the primary EDX data were further processed. A normalisation procedure against the silicon Kα X-ray intensity was undertaken to correct for any variations in sample thickness. We presumed that the Si concentration in the mineral should likely not be changed by the micro-organisms, since silicon is not an essential nutrient and the O-Si bond in sheet silicates is very strong. Bonneville et al's (2009) STEM-EDX data from a fungi-biotite thin section supports this assumption. The ratio of all the elemental X-ray counts to the counts for silicon should be constant in a non-altered biotite over the typical thickness range of a FIB section. The onset of the bulk biotite normalised O/Si ratio was selected as the "cell-mineral interface indicator".

3. Results and discussion

3.1. Identifying and avoiding sample preparation artefacts

FIB preparation of a thin section for TEM is illustrated in Figure 1a. Over-thinning with the ion beam and bending of the samples are major issues when preparing specimens of this size (Figure 1b, c and d). Where a sample depth of 2 or even 3 μm needs to be investigated, thin sections with parallel sides can be successfully produced (Bals et al., 2007; Schaffer et al., 2012). However, with the samples here the bacteria sections themselves are anything from 4 to 8 μm in depth, before the mineral surface is reached. Making electron-transparent sections with parallel sidewalls this deep is extremely difficult, and can result in preferential thinning before the entire section is sufficiently transparent (Figure 1b and c). This is because the profile of the ion beam itself is not parallel and this has to be accommodated by tilting the face of the section to be milled a few degrees off-axis from the incident ion beam, to get an approximately flat side to the section (Ishitani et al., 1994). As the section gets deeper, it becomes more difficult to keep the sides flat, and over-thinning of certain areas occurs. In addition, as deep sections such as these are milled thinner, they have less support, and non-rigid sections such as the cellular components of these samples can bend. Once this occurs protruding "bulges" will be milled away more quickly than the rest of the section, potentially leaving holes (Figure 1d). This can be avoided by leaving thicker sections (say 100-150 nm); however, this should be balanced against the required spatial resolution of the (S)TEM analysis. For example, the spatial resolution obtainable by EDX decreases with

increasing specimen thickness because of the increased interaction volume that generates X-rays from the incident beam in the thicker sections (Williams and Carter, 1996).

3.2. Identifying and avoiding electron beam damage in the STEM

Biotite is sensitive to damage by the high energy electron beam of the TEM (Bell and Wilson, 1981). At 300 keV, mass loss occurs as an exponential function of accumulated electron fluence, with lower beam current, larger beam diameters and thicker specimens all reducing the loss of elements (Ma et al., 1998) and this is therefore a major concern when using the focused probe of a STEM (operating at 197 keV in our case). Ma et al., (1998) show that the exposure of biotite to a focussed electron probe can result in hole-drilling, the rates of elemental loss are orientation dependent, with K-loss always significant and Fe, Al, Ti and Mg-loss only apparent when the specimen plane is perpendicular to (001) i.e., in the orientation used in our study, and that the rate of this element loss is not significantly reduced when the specimen is analysed in a liquid nitrogen cooled holder Thus, they suggest the main mechanisms expected for loss of elements in biotite are likely sputtering and 'diffusion'. Sputtering is a surface process that would occur at incident energies above the threshold for the displacement of surface atoms but to the best of our knowledge there are no reports of an incident energy threshold for damage of biotite. There are however reports of a threshold dose for (100 keV) electron beam induced damage of minerals such as vermiculite (Baumeister and Hahn, 1976) but again not, to the best of our knowledge, for the biotite used here. We have therefore undertaken STEM line scans on a FIB section to explore whether there is a working electron fluence (at 197 keV) that does not significantly damage the biotite. We employed three beam conditions (Table 1) to record linescans at fluences between 1.2 and 3×10^4 electrons nm^{-2} per pixel dwell point (probe settings 1, 2 and 3 in Figure 2).

For one of these three electron beam conditions, a transition occurred from beam damage (evident by mass loss, or "hole-drilling") to contamination build up (probe setting 3, Figure 2). This could occur when the hydrocarbon contamination rate exceeds the rate of sputtering or mass loss such that contamination build up on the specimen surface provides a coating that inhibits further mass loss (Egerton et al., 2010). EDX linescans were therefore recorded at a fluence rate below this transition threshold (using electron probe 4, Table 1). Under these conditions, EDX spectra were collected by scanning the same line on an area of biotite over a 30 min period without any detectable variation in the elemental composition of the biotite (as described in the methodology).

3.3. The cell-mineral interface

A well prepared cell-mineral FIB section is shown in Figure 3. Diffraction contrast is visible across the whole mineral section and does not show any obvious strain in the mineral underneath the bacteria. Selected area diffraction shows the bulk of the mineral to be crystallographically intact and atomic lattice imaging of the mineral-bacteria interface shows the top surface of the biotite to be atomically sharp and unaltered (Figure 4). A low loss EELS spectrum taken from the area at the interface used for the EF-TEM analysis gave a t/λ value of 0.92, suggesting a specimen thickness of ~ 150 nm.

STEM-EDX linescans collected with a contaminating rather than hole drilling electron beam (probe 4, Table 1) showed no elemental alteration of the biotite underneath the bacteria except in the case of Fe, where there was potentially some depletion in the first 5 nm into the biotite (Figure 5). The other elemental counts do not exhibit any detectable depletion at the biotite surface. It is possible that the activity of the growing cyanobacterial cells induced iron depletion of the surface layers of the biotite, but at this resolution the finite diameter of the electron beam should be accounted for as this could blur an elementally abrupt interface, i.e. the apparent Fe depletion may be an artefact. One way to measure the effective width of the electron beam is to use the cumulative STEM annular dark-field image intensity profile that accompanies the elemental linescans collected using the Oxford Instruments ISIS software. If we assume the bacterium-biotite interface to be atomically abrupt (consistent with Figure 4), any blurring of the STEM ADF image of the interface would purely be a result of the finite width of the electron beam and in this case the width of the transition from the cyanobacteria (low ADF intensity) to the biotite (high ADF intensity) is approximately 15 nm (intensity profile not shown). Image features smaller than the total width of the beam still might be resolved because the beam itself has a Gaussian-like intensity profile (due to the emission profile of the electron source and the round condenser lenses); however, determination of elemental depletion is not then unequivocal. Only further compositional data with a drop in Fe/Si ratio larger than three times the standard deviation of the "bulk" biotite ratio and across a width at least twice that of the working electron beam diameter would really confirm this depletion. Here, improved counting statistics could be achieved with a finer probe size and closer dwell points or longer dwell times, provided any increase in electron fluence per dwell-point remained below the contamination build up to mass loss transition already demonstrated for biotite.

EF-TEM elemental jump ratio images of carbon (K-edge), silicon ($L_{2,3}$-edge) and iron ($L_{2,3}$-edge) were also collected from the same section (Figure 6). Jump ratios were used

because of the increased elemental sensitivity over the more quantitative three window elemental maps and because of the difficulty in obtaining a reliable Si $L_{2,3}$-edge three window map due to the presence of the Al $L_{2,3}$-edge in the Si $L_{2,3}$- pre-edge region (three window maps needing more space in the pre-edge region for two windows, to accurately measure the background contribution underneath the edge) (Brydson, 2001). Once the images were collected, compositional gradients were measured using the technique outlined by Hellmann et al. (2003). In our case intensity profiles were taken across the image of the interface, integrated over 300 pixels along the interface, using Digital Micrograph software and the width of the compositional gradient was measured between the two intensity plateaus in the profiles (insets in Figure 6). Elemental gradient widths for carbon, silicon and iron were measured as 6.3, 7.2 and 6.2 nm respectively. In theory, the spatial resolution of this technique can exceed that of the STEM linescan technique. In practice though, the resolution will suffer from slight variations in focus of the image, the inherent poor signal to noise in the jump ratios and imperfect overlaying of the two filtered images. The result gives carbon and silicon interfaces of similar breadth to iron suggesting an elemental resolution of no better than 6-7 nm for the current instrumental set-up.

If weathering had occurred, the formation of vermiculite zones within the altered biotite would be one of the main structural changes expected. This is easily observed through TEM lattice imaging, as it results in an expansion of the biotite (001) lattice planes from approximately 1 to 1.4 nm as well as the formation of distinctive banding resulting from diffraction contrast generated by the expansion (Banfield and Eggleton, 1998). No such features were observed in the biotite underneath the cyanobacterial filament examined here (Figures 3 and 4). Indeed, this observation is in stark contrast to a biotite incubated underneath an ectomycorrhizal fungi hyphal which shows clear evidence of crystallographic alteration by biomechanical forcing of the hyphal tip (Bonneville et al., 2009). In addition, no chemical alteration of the biotite underneath the cyanobacterial filament was detected via EDX (Figure 5) or EELS (Figure 6) within the resolution limitations described above. In other studies, weathering of biotite by lichen has been shown to result in a depletion of potassium (Wierzchos and Ascaso, 1998), and the study by Bonneville et al. (2009) showed depletion of potassium, iron, aluminium and magnesium. The potential detection of iron depletion in the surface 5 nm of the biotite studied here (Figure 5) is below the resolution limits measured here (~15 nm for EDX linescan and ~6-7 nm for EF-TEM) and could also, arguably, be described as relatively insignificant in terms of the bioweathering of biotite

observed in incubation experiments with other microorganisms (Bonneville et al., 2009 and 2011).

4. Conclusions

To the best of our knowledge, we present here the first bioweathering study employing FIB and TEM methods for investigations of the cyanobacterium-mineral interface to search for potential mineral alterations. In more general terms, it represents one of the first reports on the role of cyanobacteria in bioweathering of sheet silicate minerals on the nanometre scale. The study shows that the FIB can be used successfully for preparation of thin specimens through a cyanobacteria-mineral interface for subsequent TEM examination. Notably, this study has shown that above a STEM electron fluence threshold of between 1.2 and 3×10^4 electron nm^{-2} per dwell-point, biotite mass loss occurs through electron "hole-drilling". Below this threshold, mass loss is not detectable and only hydrocarbon contamination build-up is observed. Consistent with this, no elemental alteration of the biotite is evident in this regime.

TEM imaging and diffraction indicate the crystallography of a biotite underneath a cyanobacterial cell to be unaltered by the bacterium and the interface between the two to be atomically abrupt. STEM-EDX line scan analysis showed that iron depletion may be present in the biotite over the first 5 nm from the bacterium interface, but the data were not sufficiently significant to be confident of this. Similarly, EF-TEM jump ratio elemental maps did not show any elemental depletion beyond 6 or 7 nm from the interface, or any differences between the elements tested. Consequently any observed depletion within the first 6 nm was considered to be a result of the mapping technique. Overall therefore, the cyanobacterial strain of Hassallia byssoidea did not cause any substantial alteration of biotite after three months of incubation on its surface. More and longer time-scale bioweathering studies with cyanobacteria need to be undertaken in the future in order to elucidate the role of this group of micro-organisms in mineral weathering.

References

Bals, S., Tirry, W., Geurts, R., Yang, Z., Schryvers, D., 2007. High-quality sample preparation by low kV FIB thinning for analytical TEM measurements. Microscopy and Microanalysis 13, 80-86.

Banfield, J.F., Eggleton, R.A., 1988. Transmission electron microscope study of biotite weathering. Clays and Clay Minerals 36, 47-60.

Baumeister, W., Hahn, M., 1976. An improved method for preparing single crystal specimen supports: H_2O_2 exfoliation of vermiculite. Micron 7, 247-251.

Bell, I. A., Wilson, C. J. L., 1981. Deformation of biotite and muscovite: TEM microstructure and deformation model. Tectonophysics 78, 201-228.

Benzerara, K., Menguy, N., Guyot, F., Vanni, C., Gillet, P., 2005. TEM study of a silicate-carbonate-microbe interface prepared by focused ion beam milling. Geochimica et Cosmochimica Acta 69, 1413-1422.

Bischoff, H.W., Bold, H.C., 1963. Some soil algae from Enchanted Rock and related algal species. Phycological Studies IV. University of Texas Publication No. 6318.

Bonneville, S., Smits, M.M., Brown, A., Harrington, J., Leake, J.R., Brydson, R., Benning, L.G., 2009. Plant-driven fungal weathering: Early stages of mineral alteration at the nanometer scale. Geology 37, 615–618.

Bonneville, S., Morgan, D., Schmalenberger, A., Bray, A., Brown, A., Banwart, S.A., Benning L.G., 2011. Tree-mycorrhiza symbiosis accelerate mineral weathering: Evidences from nanometer-scale elemental fluxes at the hypha-mineral interface. Geochimica et Cosmochimica Acta 75, 6988-7005.

Brehm, U., Gorbushina, A., Mottershead, D., 2005. The role of microorganisms and biofilms in the breakdown and dissolution of quartz and glass. Palaeogeography, Palaeoclimatology, Palaeoecology 219, 117-129.

Brydson, R., 2001. Electron Energy Loss Spectroscopy, first ed. Taylor and Francis (Garland Science).

Burford, E.P., Fomina, M., Gadd, G.M., 2003. Fungal involvement in bioweathering and biotransformation of rocks and minerals. Mineralogical Magazine 67, 1127-1155.

Büdel, B., Weber, B., Kühl, M., Pfanz, H., Sültermeyer, D., Wessels, D., 2004. Reshaping of sandstone surfaces by cryptoendolithic cyanobacteria: Bioalkalization causes chemical weathering in arid landscapes. Geobiology 2, 261-268.

Chizhikova, N.P., Omarova, E.O., Lobakova, E.S., Zenova, G.M., Manucharov, A.S., 2009. Crystallochemical transformation of phyllosilicates under the impact of cyanobacteria and actinomycetes. Eurasian Soil Science 42, 69-74.

Egerton, R.F., McLeod, R., Wang, F., Malac, M., 2010. Basic questions related to electron-induced sputtering in the TEM. Ultramicroscopy 110, 991-997.

Gadd, G.M., 2007. Geomycology: Biogeochemical transformations of rocks, minerals, metals and radionuclides by fungi, bioweathering and bioremediation. Mycological Research 111, 3-49.

Garcia-Pichel, F., 2006. Plausible mechanisms for the boring on carbonates by microbial phototrophs. Sedimentary Geology 185, 205-213.

Garcia-Pichel, F., Ramirez-Reinat, E., Gao, Q., 2010. Microbial excavation of solid carbonates powered by P-type ATPase-mediated transcellular Ca^{2+} transport. Proceedings of the National Academy of Sciences 107 (50), 21749-21754.

Gorbushina, A.A., 2007. Life on the rocks. Environmental Microbiology 9, 1613-1631.

Gorbushina, A.A., Palinska, K.A., 1999. Biodeteriorative processes on glass: Experimental proof of the role of fungi and cyanobacteria. Aerobiologia 15, 183-191.

Heaney, P.J., Vicenzi, E.P., Giannuzzi, L.A., Livi, K.J.T., 2001. Focused ion beam milling: A method of site-specific sample extraction for microanalysis of Earth and planetary materials. American Mineralogist 86, 1094-1099.

Hellmann, R., Penisson, J.-M., Hervig, R.L., Thomassin, J.-H., Abrioux, M.-F., 2003. An EFTEM/HRTEM high resolution study of the near surface of labradorite feldspar altered at acid pH: evidence for interfacial dissolution-reprecipitation. Physics and Chemistry of Minerals 30, 192-197.

Hoffland, E., Kuyper, T.W., Wallander, H., Plassard, C., Gorbushina, A.A., Haselwandter, K., Holmström, S., Landeweert, R., Lundström, U.S., Rosling, A., Sen, R., Smits, M.M., van Hees, P.A.W., van Breemen, N., 2004. The role of fungi in weathering. Frontiers in Ecology and the Environment 2, 258-264.

Hutchens, E., Valsami-Jones, E., McEldowney, S., Gaze, W., McLean, J., 2003. The role of heterotrophic bacteria in feldspar dissolution - an experimental approach. Mineralogical Magazine 67, 1157-1170.

Ishitani, T., Tsuboi, H., Yaguchi, T., Koike, H., 1994. Transmission electron microscope sample preparation using focused ion beam. Journal of Electron Microscopy 43, 322-326.

Kalinowski, B.E., Liermann, L.J., Givens, S., Brantley, S.L. 2000. Rates of bacteria-promoted solubilisation of Fe from minerals: A review of problems and approaches. Chemical Geology 169, 357-370.

Lee, M.R., Brown, D.J., Smith, C.L., Hodson, M.E., MacKenzie, M., Hellmann, R., 2007. Characterization of mineral surfaces using FIB and TEM: A case study of naturally weathered alkali feldspars. American Mineralogist 92, 1383-1394.

Lee, M.R., 2010. Transmission electron microscopy (TEM) of Earth and planetary materials: a review. Mineralogical Magazine 74, 1-27.

Ma, C., FitzGerald, J.D., Eggleton, R.A., Llewellyn, D.J., 1998. Analytical electron microscopy in clays and other phyllosilicates: Loss of elements from a 90-nm stationary beam of 300-keV electrons. Clays and Clay Minerals 46, 301-316.

Madigan, M.T, Martinko, J.M., Parker, J. 2003. Brock biology of microorganisms, tenth ed. Prentice Hall, Upper Saddle River, New Jersey.

Obst, M., Gasser, P., Mavrocordatos, D., Dittrich, M., 2005. TEM-specimen preparation of cell/mineral interfaces by focused ion beam milling. American Mineralogist 90, 1270-1277.

Olsson-Francis, K., Cockell, C.S., 2010. Use of cyanobacteria for in-situ resource use in space applications. Planetary and Space Science 58, 1279-1285.

Pan, Y., Brown, A., Brydson, R., Warley, A., Li, A., Powell, J. 2006. Electron beam damage studies of synthetic 6-line ferrihydrite and ferritin molecule cores within a human liver biopsy. Micron 37, 403-411.

Schaffer, M., Schaffer, B., Ramasse, Q., 2012. Sample Preparation for atomic-resolution STEM at low voltages by FIB. Ultramicroscopy 114, 62-71.

Wierzchos, J., Ascaso, C., 1998. Mineralogical transformation of bioweathered granitic biotite, studied by HRTEM: Evidence for a new pathway in lichen activity. Clays and Clay Minerals 46, 446-452.

Williams, D.B., Carter, C.B., 1996. Transmission Electron Microscopy. Plenum Press, New York.

Wirth, R., 2009. Focused ion beam (FIB) combined with SEM and TEM: Advanced analytical tools for studies of chemical composition, microstructure, and crystal structure in geomaterials on a nanometre scale. Chemical Geology 261, 217-229.
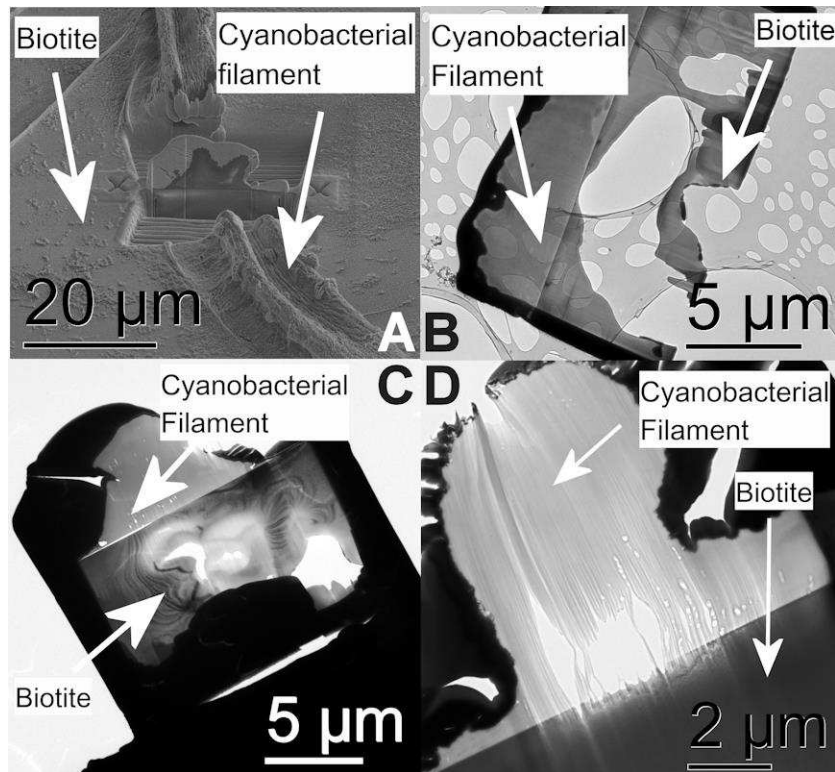
Figure 1. A) SEM image of a FIB-prepared cross-section of a cyanobacterial filament-biotite interface. TEM images of ion beam damage of the mineral and cyanobacteria cross-sections by B) over-thinning the base of the lamella, C) over-thinning the whole section and D) over-thinning protruding parts of the section.
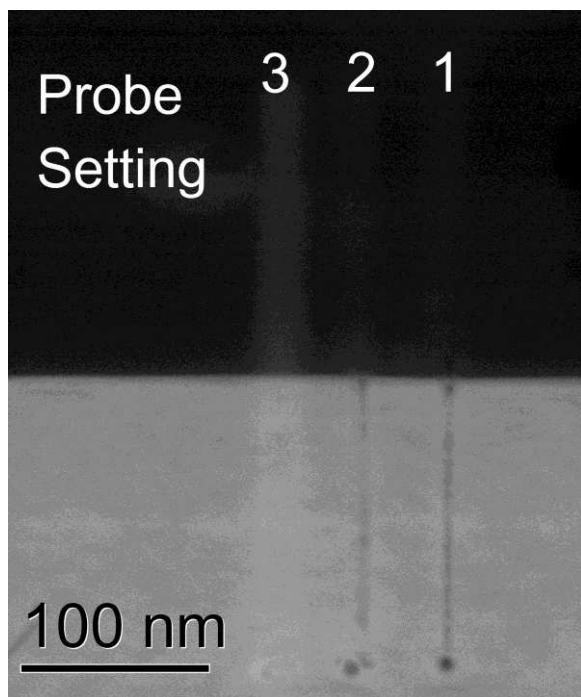
Figure 2. HAADF STEM image of a biotite-cyanobacterium interface after line-scanning across the interface with progressively lower electron fluence per dwell-point electron beams. A transition from hole-drilling to contamination build up on the biotite is seen when the electron fluence per dwell-point drops from that in probes 1 and 2 to that in probe 3 (fluences and probe sizes are detailed in Table 1).
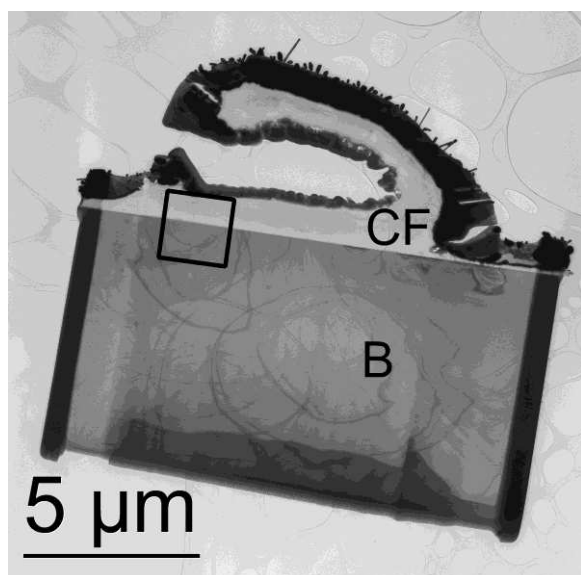
Figure 3. Bright field TEM image of a well-prepared, FIB section of the biotite-cyanobacterium interface. The "even" diffraction contrast in the image of the biotite (B) indicates that there is little structural alteration of the mineral immediately next to the interface (cyanobacterial filament indicated by CF). The region used for the collection of both the EDX linescan data presented in Figure 5 and the EF-TEM data presented in Figure 6 is marked with a black square.

16
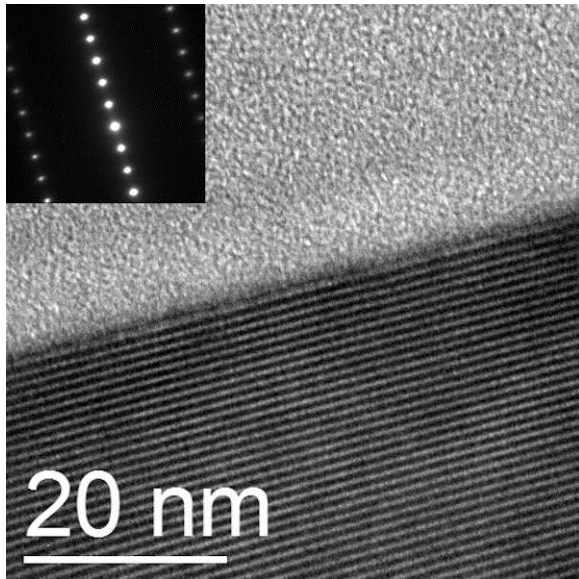
Figure 4. TEM image at the interface of the biotite-cyanobacterium section in Figure 3. The (001) lattice plane spacing of the biotite directly underneath the interface is a constant and unaltered 1 nm and this is confirmed by the inset electron diffraction pattern.
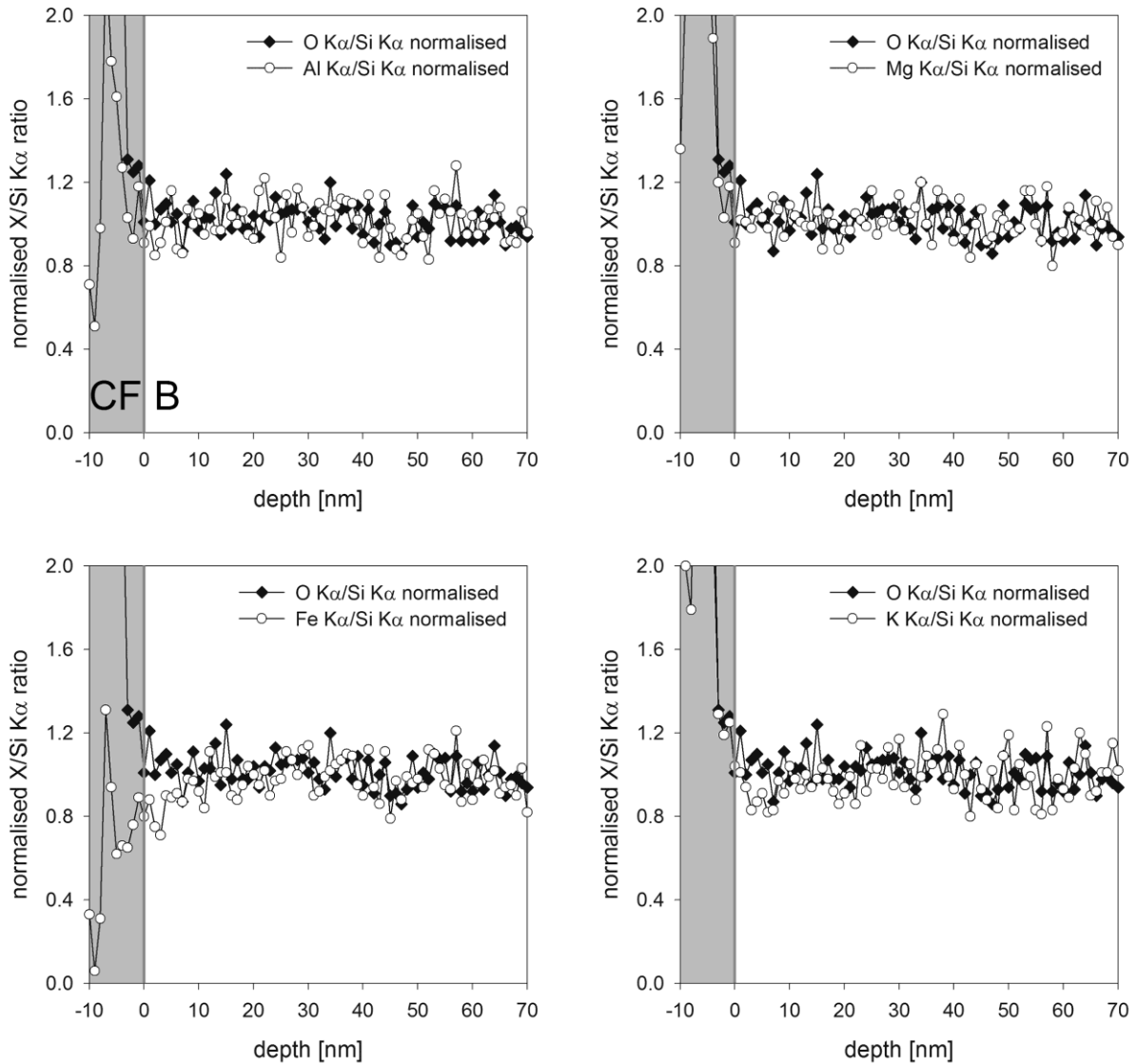
Figure 5. STEM-EDX linescans across the interface of the biotite-cyanobacterium section in Figure 3. The grey regions in the plots correspond to the cyanobacterium (CF) and the white to the biotite (B). The elemental signals are normalised to the Si-Kα X-ray count to accommodate for variations in specimen thickness. Only the Fe/Si elemental profile shows any depletion at the surface of the biotite and it is only in the first 5 nm, which is less than the estimated diameter of the STEM electron beam (~15 nm).
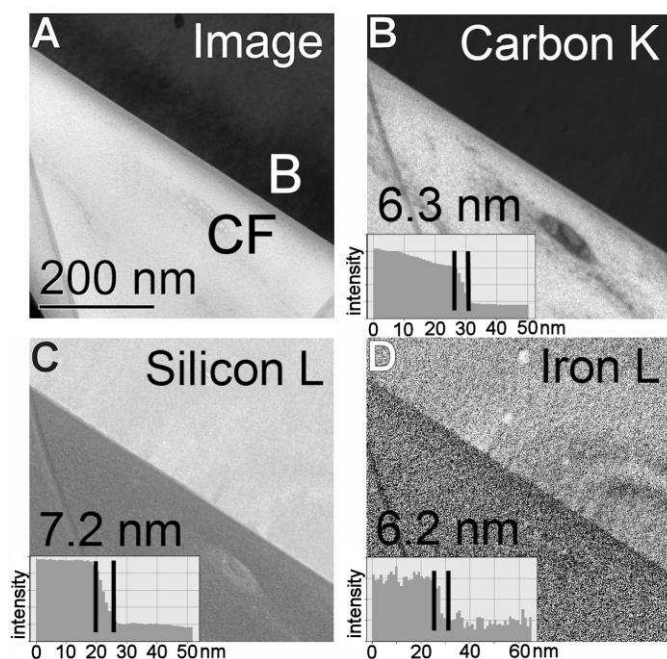
Figure 6. A) Zero loss filtered TEM image at the interface of the biotite (B)-bacterium (CF) section in Figure 3. B) Carbon (K-edge) jump ratio map of the interface in A with an intensity profile across the interface inset and an estimated interfacial width of 6.3 nm. C) Silicon ($L_{2,3}$-edge) jump ratio map of the interface in A with an intensity profile across the interface inset and an estimated interfacial width of 7.2 nm. D) Iron ($L_{2,3}$-edge) jump ratio map of the interface in A with an intensity profile across the interface inset and an estimated interfacial width of 6.2 nm.

Setting	Microscope	Extraction Voltage / kV	Condenser Aperture / μm	Spot Size Setting	Probe Diameter / nm	Fluence per dwell point / electrons nm^{-2}
1	Tecnai	4.25	100	9	7.5	1.3×10^4
2	Tecnai	3.25	70	5	11.5	3.0×10^4
3	Tecnai	3.25	70	7	9.2	1.2×10^4
4	CM200	3.25	100	5	15	1.2×10^4

Table 1. The microscope conditions, electron beam diameters (measured by STEM annular dark field intensity profiles) and electron fluences per dwell-point (measured using the procedure outlined in Pan et al., 2006) for the three probe conditions used to establish the contamination build up to mass loss threshold for STEM analysis of biotite (probes 1, 2 and 3) and the same for the probe (4) used for STEM-EDX linescan analysis across the biotite-bacterium interface (Figure 5).